ELSEVIER

Journal of Membrane Science 165 (2000) 19–29

journal of MEMBRANE SCIENCE

www.elsevier.nl/locate/memsci

A comparison of rotating and stationary membrane disk filters using computational fluid dynamics

Christophe A. Serra *, Mark R. Wiesner

Rice University, Department of Environmental Science and Engineering, 6100 Main Street, Houston, TX 77005, USA

Received 28 July 1998; received in revised form 21 June 1999; accepted 22 June 1999

Abstract

Rotating disk filters, implemented either with an impermeable disk rotating above a stationary membrane disk or with a stationary baffle next to a rotating membrane disk, are investigated numerically using a commercial computational fluid dynamics package. The fluid is assumed to be Newtonian, incompressible, non-fouling and isothermal. The κ–ϵ model is used to describe turbulent flow in the vessel surrounding the rotating disk.

For given values of the flow rate and RPM, stationary membrane disk filters require less power input. Rotating membrane disk filters produce a higher shear stress on the membrane surface which may reduce fouling but may also result in a reversed flow of permeate due to the 'back pressure' induced by centrifugal force on fluid within the membrane disk. Operating conditions and design parameters should be selected to minimize this 'back pressure' phenomenon and maximize the effective membrane available for filtration.

Keywords: Stationary membrane disk; Rotating membrane disk; Computational fluid dynamics; Turbulent flow; Filter design

1. Introduction

Membrane filtration often relies on the presence of a shear stress at the membrane surface to reduce the accumulation of foulants [1,2]. In the classical cross-flow filtration, the shear stress is brought by the tangential flow along the membrane surface but as a result leads to pressure drops. For high concentrated suspensions, the shear stress to reduce fouling may be so high that the required flow rate would induce an unacceptable pressure drop . For rotating disk filters, the shear stress and flow rate are unlinked since shear stress is only a function of the rotational speed. Therefore, these filters appear to be most applicable to the clarification of very high concentration suspensions [3–4] and the separation of biological products [5–6]. Commercially, rotating disk filters have been implemented both as membrane disks rotating between stationary baffles [7], and as fixed membrane disks next to rotating baffles [8]. The hydrodynamics of these membrane filters are expected to be greatly affected by any variation in operating conditions (flow rate, RPM) and geometry parameters (disk radius, clearance between membrane and baffle). However, there are few guidelines in the literature for the design of such filters.

This work deals with the use of computational fluid dynamics (CFD) to investigate and compare the performance of rotating membrane disk filters (RMDFs)

* Corresponding author. Present address: Ecole de Chimie, Polymères et Matériaux, Département Polymères, 25 rue Becquerel, 67087 Strasbourg Cedex 2, France; Tel.: +33-388-13-69-25; fax: +33-388-13-69-23.
E-mail address: serrac@ecpm.u-strasbg.fr (C.A. Serra).

0376-7388/00/$ – see front matter
PII: S0376-7388(99)00219-7

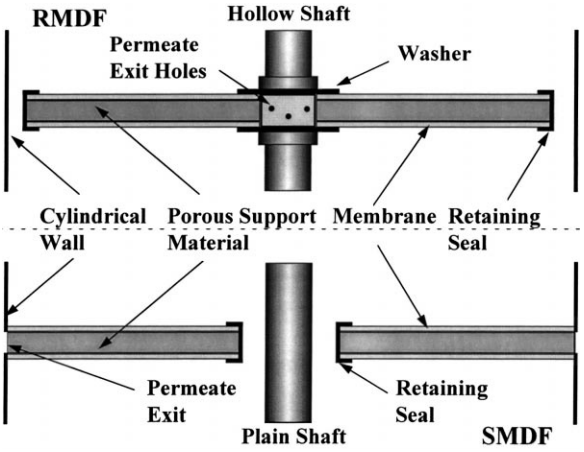

Fig. 1. View of the membrane disks.

and stationary membrane disk filters (SMDFs) over a range of operating conditions and design parameters.

2. Methodology

2.1. Filter units

In the case of the RMDF, the membrane disk is mounted on a rotating shaft via two retaining sleeves and washers. The stationary membrane disk in the SMDF configuration is mounted to the exterior wall of the vessel. The membrane disk is a porous medium with a flat microfiltration membrane on each of its faces (Fig. 1). For the purpose of symmetry, the feed inlet is assumed to be a slit around the vessel opposite to the rotating disk tip. In the RMDF configuration, the fluid flows through the membrane to the center where it exists through the hollow shaft. In the SMDF configuration, the permeate is collected at the periphery of the vessel. Both filters operate in dead-end mode. Parameter baseline values were selected to correspond to those anticipated in the laboratory and full scale units (see Table 1).

2.2. Computational fluid dynamics

A commercial CFD package, FIDAP (Fluid Dynamics International, Evanston, IL, USA), was used to model the hydrodynamics of those two rotating disk filters. Turbulence, which occurs in such geometries

Table 1
Parameter baseline values

Parameter	Value
Tank radius	7.5×10^{-2} m
Shaft radius	1.3×10^{-2} m
Clearance between disks	7.14×10^{-2} m
Membrane permeability	6.5×10^{-16} m^2
Membrane thickness	10^{-4} m
Support permeability	8.18×10^{-12} m^2
Support thickness	3.5×10^{-3} m
Baffle permeability	None
Baffle thickness	3.6×10^{-3} m
Rotating disk radius	7.1×10^{-2} m
Gap with cylindrical wall	4×10^{-3} m
Retaining seal length	10^{-2} m
Washer length	1.2×10^{-2} m
Stationary disk radius	7.5×10^{-2} m
Gap with rotating shaft	4×10^{-3} m
Retaining seal length	3.33×10^{-3} m
Filtration flux	200 l h^{-1} m^{-2}

especially at high rotational speeds, is typically modeled by either the zero-equation model based on the Prandtl mixing length or the κ–ϵ model. The CFD tool accommodates flow through porous media using the Forchheimer–Brinkman model [9]. The fluid flow equations are solved by the finite element method.

Symmetry in filter units allows the simulation domain to be reduced to a quadrant of a cut through the vessel modeled in two dimensions (Fig. 2). The reduction in the computational domain greatly facilitates modeling under turbulent conditions. The radial axis is along the stationary disk while the axial axis runs along the shaft.

In this work, the fluid is assumed to be Newtonian, isothermal and incompressible. Furthermore, steady-state solutions are calculated assuming constant membrane permeability. Thus, membrane fouling is not considered. No-slip boundary conditions are set at all solid wall boundaries (cylindrical wall, rotating shaft, washer, retaining seal and baffle). The azimuthal velocity (v_θ) on the rotating disk and shaft surface is set according to the equation:

$$v_\theta = r\omega \tag{1}$$

where r is the radial distance and ω the rotational speed. Flow in the inlet and outlet regions is assumed to be uniform. The κ–ϵ model is used to describe turbulent flow within the vessel and has been found

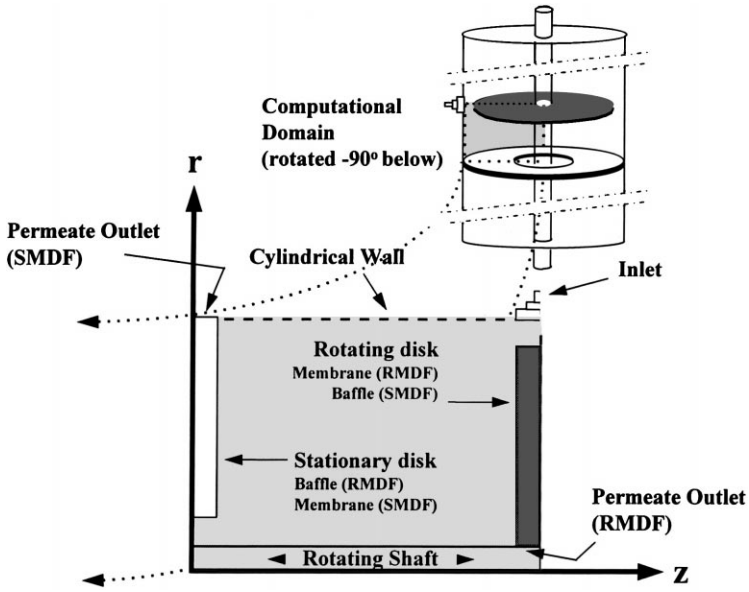

Fig. 2. Computational domain.

to yield a satisfactory representation of flow in similar geometries [10–11].

2.3. Simulations

The global transmembrane pressure (Δp_G) is defined as the difference between the inlet pressure and the permeate exit pressure (Fig. 2) and is related to the power consumption (P) required to drive the fluid through the filters:

$$P = Q_0 \Delta p_G \tag{2}$$

where Q_0 is the overall throughput flow rate. The power consumption to rotate the shafts is not considered in this study since the filters are compared for the same rotational speed.

The pressure on the feed side of the membrane surface and that on the permeate side are calculated as a function of the radial position. The difference of those two pressures is defined as the local transmembrane pressure (Δp_L). Knowing this pressure difference along the membrane, one can evaluate the dimensionless cumulative flow rate (Q^*) as the permeate flow rate through the membrane from the edge of the washer (RMDF) or retaining seal tip (SMDF) to a radial distance 'r' over the overall throughput flow rate (Q_0):

$$Q^*(r) = \frac{\int_{r_0}^{r} 2\pi (L_p/\mu e) r \Delta p_L(r) \mathrm{d}r}{Q_0} \tag{3}$$

where r_0 is the radial position of the washer edge or retaining seal tip, e the membrane thickness, L_p the membrane permeability and μ the permeate viscosity. Increases in the dimensionless cumulative flow rate with r indicate that increments in membrane area by increasing disk radius produce additional flow.

The code used in this study has been validated by Engler [12] by comparing the global transmembrane pressures returned by simulations and those obtained from experiments to achieve a specific flux. The discrepancy was found to be less than 7% so that the code could be considered accurate enough to be used as an assessment tool.

3. Results and discussion

3.1. Flow pattern within the filters

Under the influence of disk rotation, the fluid moves radially outward along the rotating disk and

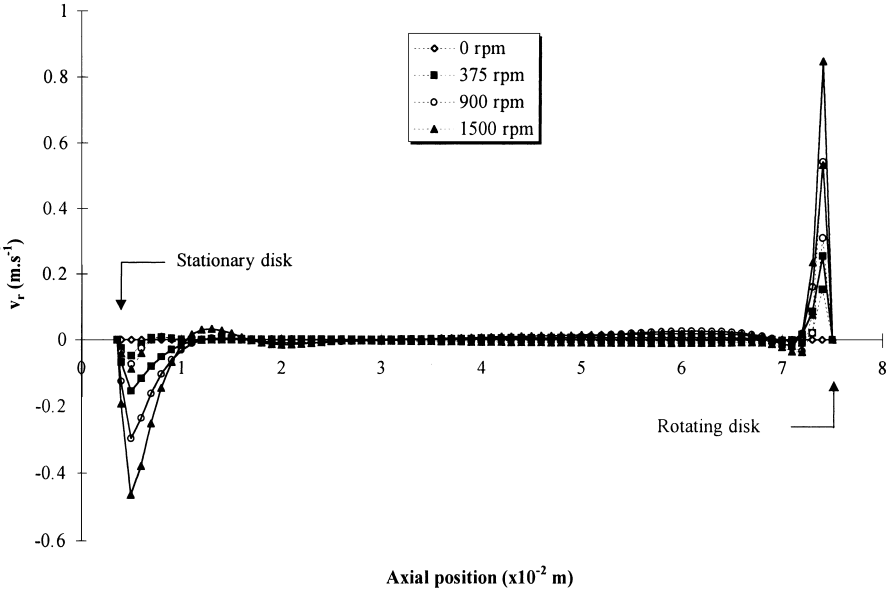

Fig. 3. Variation of the radial velocity across the filters as a function of the RPM at a radial distance of 4.3×10^{-2} m for RMDF and 6.26×10^{-2} m for SMDF (—: SMDF; ----: RMDF).

returns inward in the vicinity of the stationary disk (Fig. 3). Variations in the azimuthal velocity indicate that the boundary layers on the stationary and rotating disks remain close to those surfaces leading to a core fluid which rotates nearly as a solid body with a rotational speed smaller than that of the rotating disk (Fig. 4). The fluid entering the vessel flows along the cylindrical wall towards the stationary disk where it

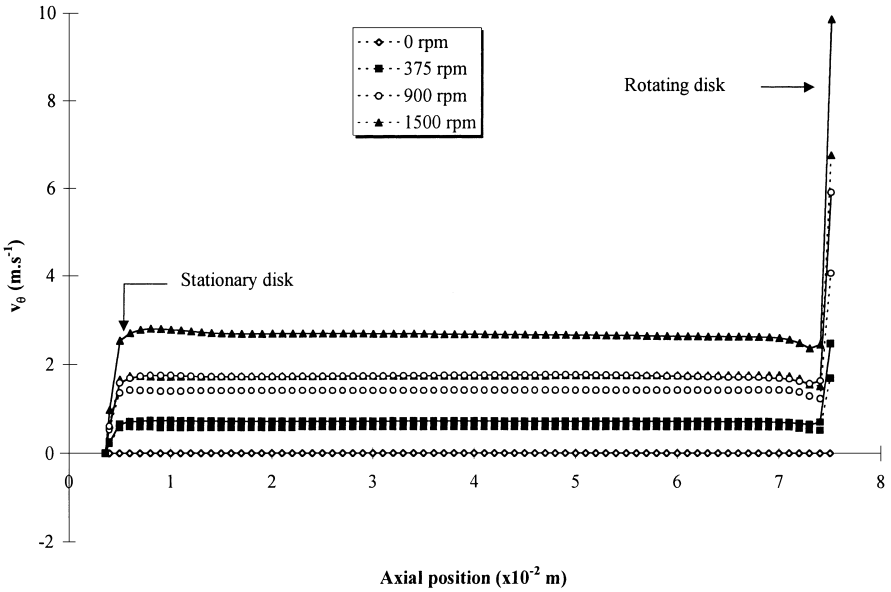

Fig. 4. Variation of the azimuthal velocity across the filters as a function of the RPM at a radial distance of 4.3×10^{-2} m for RMDF and 6.26×10^{-2} m for SMDF (—: SMDF; ----: RMDF).

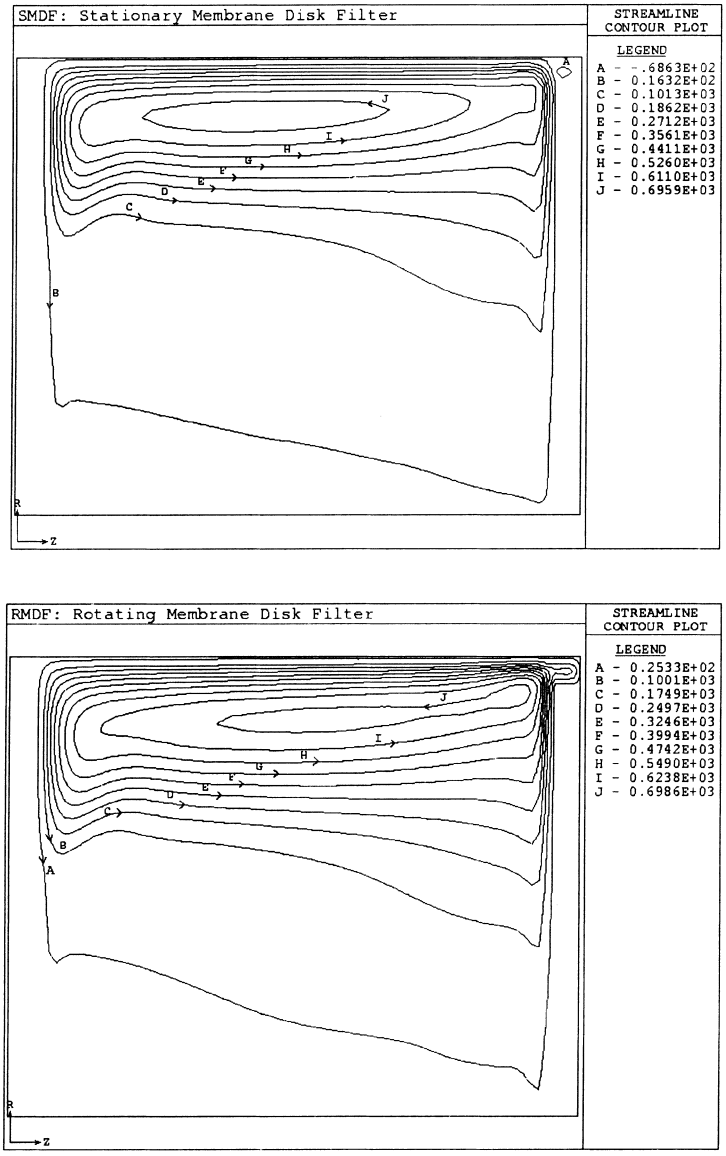

Fig. 5. Streamlines and subsequent values of the stream function at 1500 RPM for the SMDF (top) and RMDF (bottom).

moves radially to the shaft. The fluid then returns axially towards the rotating disk to compensate the fluid thrown radially away by centrifugal force as shown in Fig. 5. The streamline contour represents basically the curves (streamlines) traced out by a fluid element. Each curve is actually a line of iso-stream function from which the direction of the flow can be deduced [13]. A zone of internal circulation with a high velocity appears in the upper portion of the chamber close to the membrane surface. This recirculation flow pattern has been previously described by Daily and Nece [14] and more recently by Rudniak and Wronski [15] in the case of non-porous disks. Due to the relatively small permeability, characteristic of membrane filtration, the overall flow pattern is dominated by disk rotation.

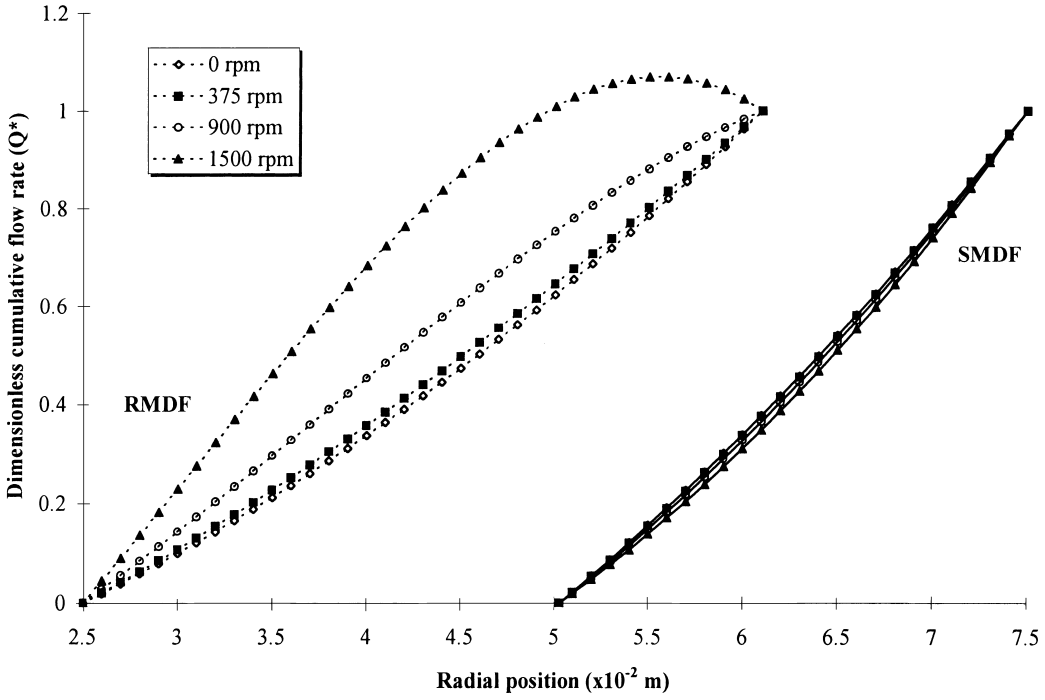

Fig. 6. Variation of the dimensionless cumulative flow rate along the membrane as a function of the RPM (—: SMDF; ----: RMDF).

3.2. Effect of the rotational speed on membrane performance

The membrane performance expressed as the variation of the dimensionless cumulative flow rate with respect to the radial position is shown for each filter in Fig. 6. As expected, the dimensionless cumulative flow rate increases along the membrane. However, while the SMDF is scarcely affected by any variation in the RPM, the RMDF exhibits strong deviations. Hence, for the higher RPM, the dimensionless cumulative flow rate passes through a maximum. A portion of the membrane is submitted to a reversed flow with some of the permeate returning to the feed compartment due to a reversal in the sign of transmembrane pressure. In the permeate compartment, the pressure reflects a balance between pressure loss through the disk medium and membrane and the centrifugal force effects. The centrifugal force (f_v) due to disk rotation acting on the fluid inside the support is proportional to the square of the rotational speed and the radial position:

$$f_v = \rho r \omega^2 \quad (4)$$

where ρ is permeate density. Therefore, at large radial positions and high rotational speeds, the centrifugal force effects are higher than the pressure loss effects resulting in local permeate pressure which is higher than the feed side pressure and in a negative local transmembrane pressure. In addition to reducing the effectiveness of installed membrane area, this 'back pressure' phenomenon might also damage the membrane over time since forces acting in an opposite direction could potentially tear the membrane from its support.

Pressure on the permeate side increases due to centrifugal force effects requiring a higher global transmembrane pressure to drive the same amount of fluid across the membrane and through the porous support. Therefore, the RMDF exhibits a higher global transmembrane pressure and is more affected by variations in RPM (Fig. 7). For instance, at 1500 RPM, the SMDF is calculated to have a global transmembrane pressure which is 68% less than that in

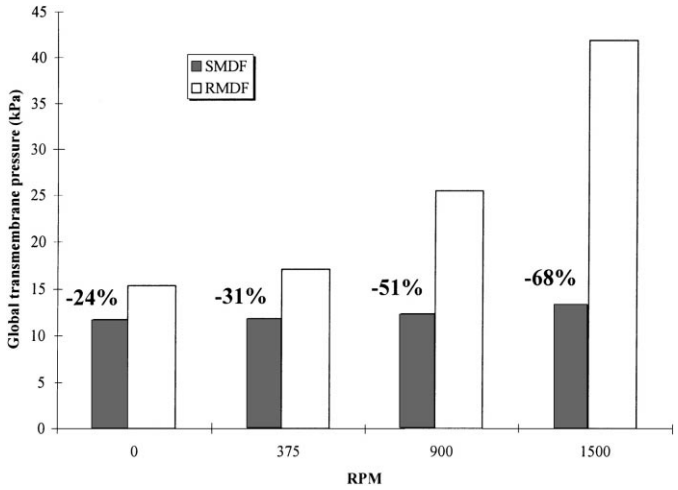

Fig. 7. Global transmembrane pressure as a function of the RPM. Percentages give the reduction for SMDF in comparison with RMDF.

the RMDF. As a result, power consumption is expected to be smaller when the membrane disk is fixed.

However, as shown in Fig. 8, shear stresses on the surface of the SMDF membrane are significantly less and more uniform than those on the RMDF membrane. On the rotating membrane disk, the shear stress varies linearly with respect to the radial position and increases with the RPM. The shear stress is imposed by the azimuthal velocity gradient across the boundary layer which is a function of radial position and rotational speed [16]. A higher shear stress may reduce fouling leading to a lower global transmembrane pressure over time [1,2,4].

The remaining results presented here assume a rotational speed of 1500 RPM.

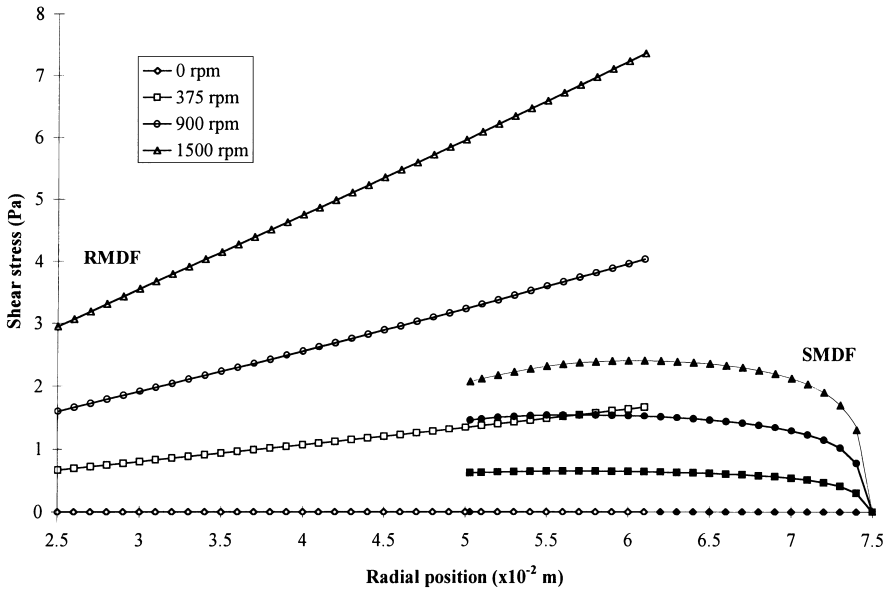

Fig. 8. Variation of the shear stress along the membrane as a function of the RPM (—: SMDF; - - - -: RMDF).

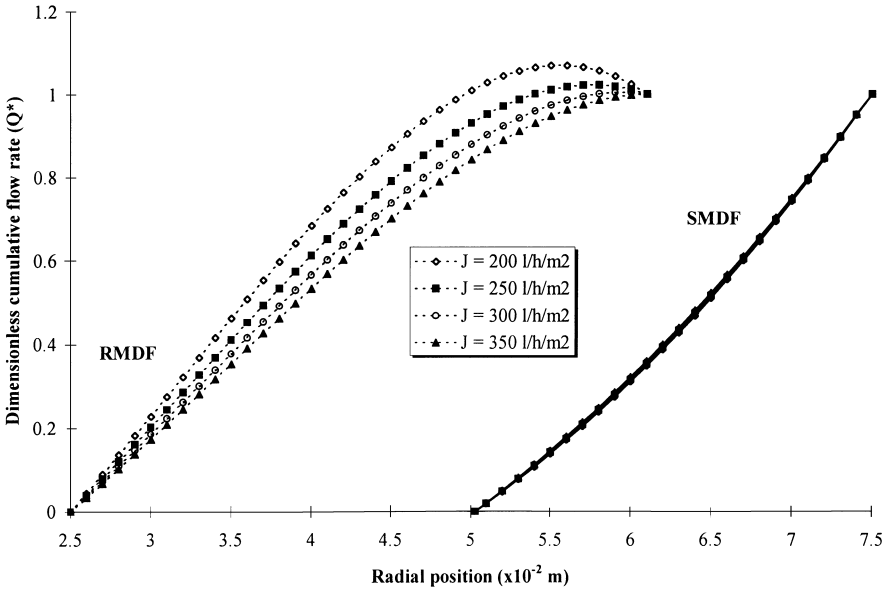

Fig. 9. Variation of the dimensionless cumulative flow rate along the membrane as a function of filtration flux (—: SMDF; ----: RMDF).

3.3. Reducing the 'back pressure'

Increases in filtration flux reduce the effects of a local 'back pressure' at the membrane disk extremity (Fig. 9). Increasing the filtration flux leads to an increased feed side pressure. Pressure loss through the disk support also increases. However, the centrifugal force is only a function of r and ω (see Eq. (4)). Therefore, there is a value of the filtration flux for which the 'back pressure' effect is overwhelmed. As dictated

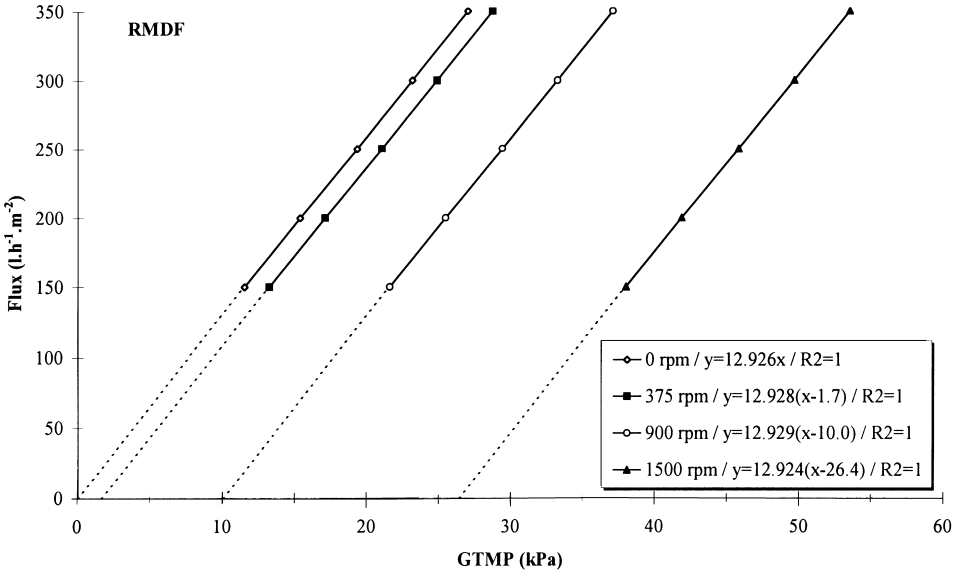

Fig. 10. Variation of filtration flux as a function of the global transmembrane pressure for the RMDF.

by Darcy's law, the filtration flux varies linearly as a function of the global transmembrane pressure (Fig. 10). Yet, one can remark that, except for the case of no rotation, those lines do not pass through the origin. The *x*-intercept is a measure of the global back pressure (p_{bck}) which must be overcome to initiate the filtration. As previously discussed, global back pressure increases with RPM. For example, global back pressures of 1.7, 10 and 26.4 kPa were calculated at RPMs of 375, 900 and 1500, respectively yielding the following correlation between global back pressure and the square of the rotational speed ($R^2 = 0.99$).

$$p_{bck} = 1.18\,\omega^2 \quad (5)$$

The 'back pressure' can also be reduced by decreasing the membrane area (Fig. 11). A reduction in the filtration area is achieved by using smaller rotating disks. Since the radial position of the membrane tip is smaller, the centrifugal force is reduced (Eq. (4)). Also the feed side pressure increases.

Membrane permeability is found to have a large effect on 'back pressure' (Fig. 12); higher permeabilities generate a higher 'back pressure'. As permeability increases, less pressure is required to flow the same amount of fluid through the membrane. Hence, the pressure on the permeate side may more easily exceed the feed pressure. Filters with high permeability should therefore be designed to operate at either a higher flow rate or a smaller membrane area.

3.4. Effect of fluid viscosity and clearance between disks

During filtration, the fluid viscosity within the vessel may increase as the concentration of retained particles increases. While membrane performance (i.e. local and global transmembrane pressure) appears to be relatively insensitive to fluid viscosity, the shear stress on the membrane surface is greatly affected by viscosity. An increase in viscosity reduces shear stress. Therefore, to maintain a shear stress high enough to avoid particle deposition, it may be necessary to increase the RPM during the filtration.

An important design parameter is the clearance between the rotary and stationary disk since clearance is related to the amount of membrane area per unit of vessel volume (packing density). For the smallest clearance studied (1.14×10^{-2} cm), no significant change in membrane performance was calculated to occur. However, clearance affects the shear stress significantly. Reduction in clearance is predicted to result in a decrease in the shear stress on the membrane sur-

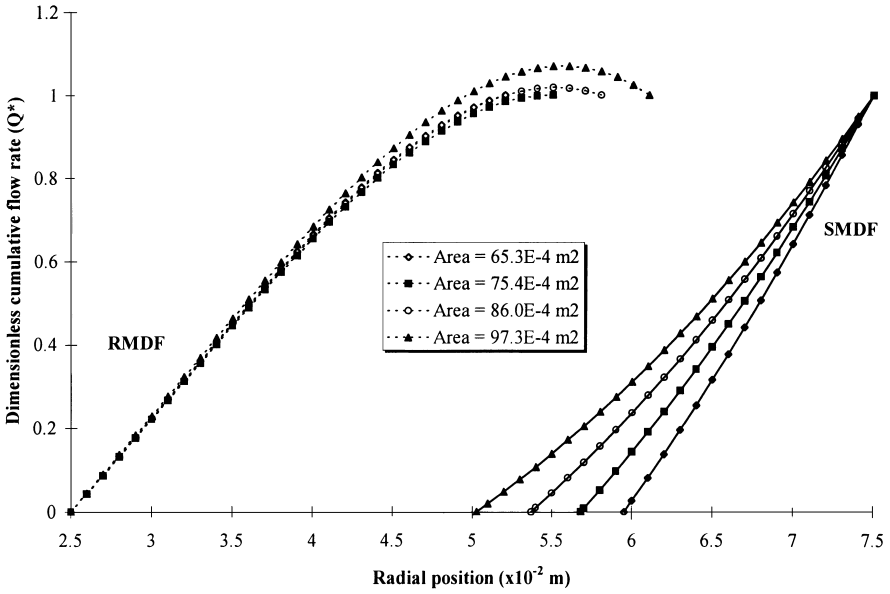

Fig. 11. Variation of the dimensionless cumulative flow rate along the membrane as a function of membrane area (—: SMDF; - - - -: RMDF).

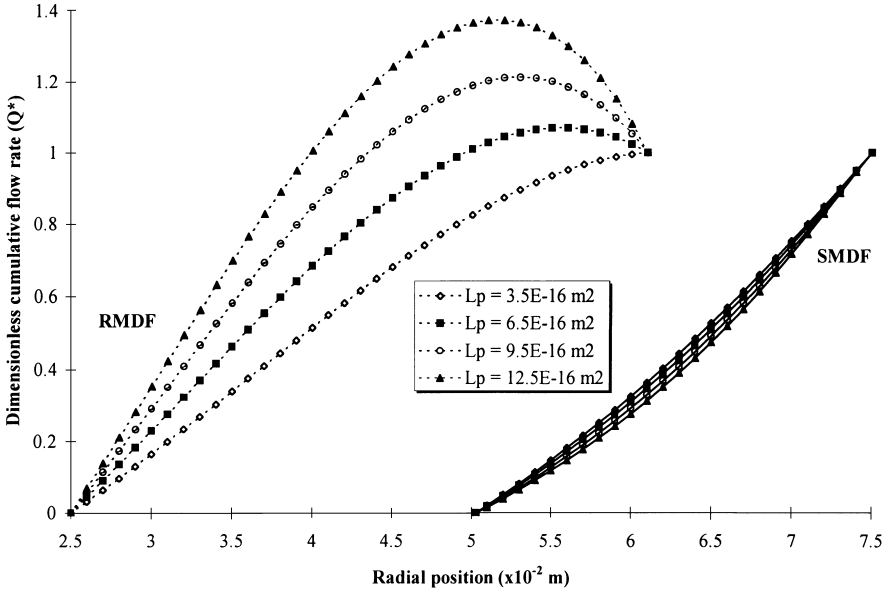

Fig. 12. Variation of the dimensionless cumulative flow rate along the membrane as a function of membrane permeability (—: SMDF; ----: RMDF).

face for the RMDF while producing an increase for the SMDF. As the distance between the rotating and the stationary disk is reduced, the two boundary layers tend to merge and so the shear stresses approach the same value.

4. Conclusions

For a given flow rate and RPM, RMDFs are calculated to provide the highest shear stress on the membrane surface but with a subsequently higher global transmembrane pressure compared with SMDFs. Fluid viscosity and clearance between disks have almost no effect on local and global transmembrane pressure and therefore do not significantly change membrane performance with respect to non-fouling fluid flow. However, the shear stress on the membrane surface is greatly affected by clearance and viscosity. Shear stress decreases as viscosity increases. A decrease in the clearance leads to an increase in the shear stress for the SMDF and a decrease in shear stress on the RMDF membrane surface.

For RMDFs, results show that the centrifugal force due to rotation may locally increase the permeate side pressure above the feed side pressure resulting in a reversed flow of permeate. To initiate the permeation, the global transmembrane pressure must be greater than a threshold value which is correlated with the square of the rotational speed (Eq. (5)). This 'back pressure' phenomenon can be reduced by reducing the membrane disk diameter, decreasing membrane permeability or increasing the feed flow rate.

Although there appears to be some advantage to SMDF configuration based on energy consumption, this advantage is not likely to persist if fouling occurs since the deposition of foulants will quickly change the global transmembrane pressure.

5. List of symbols

5.1. Latin notation

e	membrane thickness (m)
f_v	volumetric force ($N\,m^{-3}$)
J	filtration flux ($l\,h^{-1}\,m^{-2}$)
L_p	permeability coefficient (m^2)
P	power consumption (W)
p_{bck}	global back pressure (Pa)
Q^*	dimensionless cumulative flow rate (–), Eq. (3)

Q_0 overall throughput flow rate ($m^3\,s^{-1}$)
r radial position (m)
R R^2 value (–)
r_0 radial position of the edge of washer (RMDF) or retaining seal tip (SMDF) (m)
v velocity ($m\,s^{-1}$)
z axial position (m)

5.2. Greek symbols

θ azimuthal position (rad)
μ dynamic fluid viscosity (Pa s)
ρ fluid density ($kg\,m^{-3}$)
ω rotational speed (s^{-1})
κ turbulent kinetic energy ($m^2\,s^{-2}$)
ϵ viscous dissipation rate of turbulent kinetic energy ($m^2\,s^{-3}$)
Δp_G global transmembrane pressure (Pa)
Δp_L local transmembrane pressure (Pa)

5.3. Subscript

θ azimuthal component
r radial component
z axial component

References

[1] A.S. Jönsson, Influence of shear rate on the flux during ultrafiltration of colloidal substances, J. Membr. Sci. 79 (1993) 93–99.
[2] M.C. Aubert, M.P. Elluard, H. Barnier, Shear stress induced erosion of filtration cake studied by a flat rotating disk method: Determination of the critical shear stress erosion, J. Membr. Sci. 84 (1993) 229–240.
[3] N. Ohkuma, T. Shinoda, T. Aoi, Y. Okaniwa, Y. Magara, Performance of rotating disk modules in a collected human excreta treatment plant, Wat. Sci. Tech. 30(4) (1994) 141–149.
[4] J.A. Engler, M.R. Wiesner, C. Anselme, Treatment of PAC slurry using rotating disk membrane, In Proc. of 1995 Membrane Technology Conference, Reno, NV, USA, vol. 1, 1995, pp. 747–758.
[5] S.S. Lee, A. Burt, G. Russotti, B. Buckland, Microfiltration of recombinant yeast cells using disk dynamic filtration system, Biotechnol. Bioeng. 48 (1995) 386–400.
[6] U. Frenander, A.S. Jönsson, Cell harvesting by cross-flow microfiltration using a shear-enhanced module, Biotechnol. Bioeng. 52 (1996) 397–403.
[7] SpinTek introduces small centrifugal crossflow ultrafiltration system, Membrane and Separation Technology News 10 (12) (1992).
[8] B. Culkin, A. Plotkin, M. Monroe, Solve membrane fouling problems with high-shear filtration, Chem. Eng. Prog., (1998) 29–33.
[9] Theory manual of FIDAP 7.0, Fluid Dynamics International, Evanston, IL, USA, pp. 2.31–2.39.
[10] J.W. Chew, Computation of Flow and Heat Transfer in Rotating Disc System, Theoretical Science Group, Rolls Royce, Derby, UK, 1987.
[11] M. Williams, W.C. Chen, G. Bache, A. Eastland, Methodology of internal swirling flow systems with a rotating wall, J. Turbomachinery 113 (1991) 83–90.
[12] J.A. Engler, Investigation of membrane filtration in a rotating disk geometry: use of computational fluid dynamics and laboratory evaluation, Doctoral thesis, Rice University, Houston, TX, USA, 1997.
[13] R.B. Bird, W.E. Stewart, E.N. Lightfoot, Transport Phenomena, Wiley, New York, 1980.
[14] J.W. Daily, R.E. Nece, Chamber dimension effects on induced flow and frictional resistance of enclosed rotating disks, Trans. ASME: J. Basic Eng., 1960 pp. 217–232.
[15] L. Rudniak, S. Wronski, Laminar flow hydrodynamics of rotating dynamics filters, Chem. Eng. J. 58 (1995) 145–150.
[16] H. Schlichting, Boundary-layer Theory, McGraw-Hill, New York, 1968.